Gas transport behavior of mixed-matrix membranes composed of silica nanoparticles in a polymer of intrinsic microporosity (PIM-1)

Ahn, Juhyeon; Chung, Wook-Jin; Pinnau, Ingo; Song, Jingshe; Du, Naiying; Robertson, Gilles P.; Guiver, Michael D.

Publisher's version / Version de l'éditeur:
https://doi.org/10.1016/j.memsci.2009.09.047
Journal of membrane science, 346, January 2, pp. 280-287, 2010

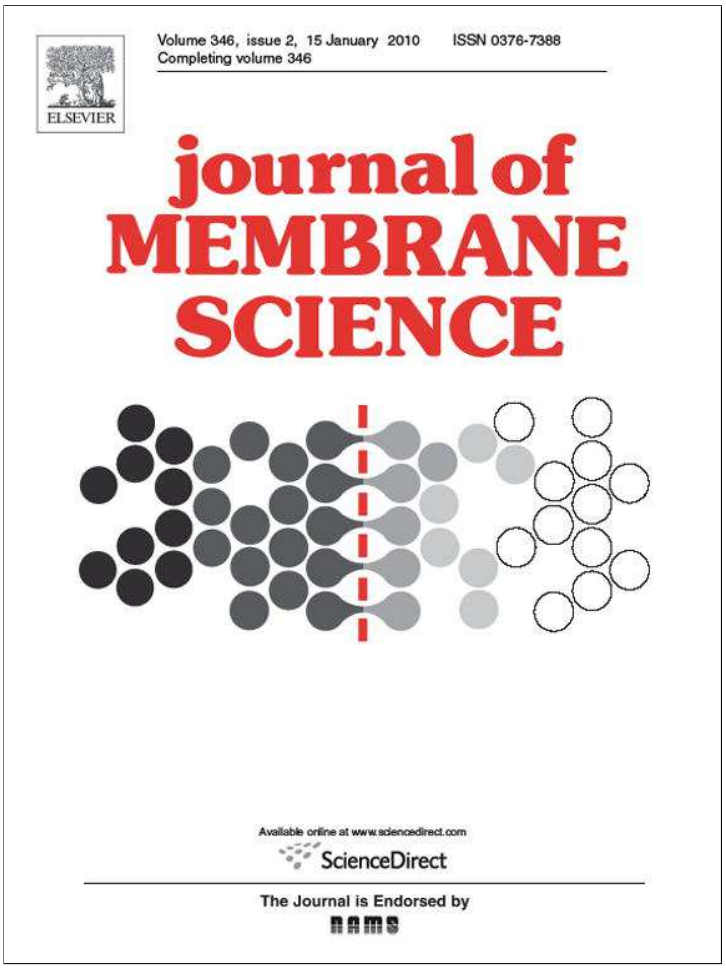

Journal of Membrane Science 346 (2010) 280–287

Contents lists available at ScienceDirect

Journal of Membrane Science

journal homepage: www.elsevier.com/locate/memsci

Gas transport behavior of mixed-matrix membranes composed of silica nanoparticles in a polymer of intrinsic microporosity (PIM-1)☆

Juhyeon Ahn[a,c], Wook-Jin Chung[a], Ingo Pinnau[b], Jingshe Song[c], Naiying Du[c], Gilles P. Robertson[c], Michael D. Guiver[c,*]

[a] Department of Environmental Engineering and Biotechnology, MyongJi University, San 38-2, Nam-dong, Cheoin-Gu, Yongin-Si 449-728, South Korea
[b] Membranes Research Center, King Abdullah University of Science and Technology (KAUST), Thuwal, Saudi Arabia
[c] Institute for Chemical Process and Environmental Technology, National Research Council of Canada, 1200 Montreal Road, Ottawa, ON K1A 0R6, Canada

ARTICLE INFO

Article history:
Received 2 August 2009
Received in revised form
21 September 2009
Accepted 23 September 2009
Available online 30 September 2009

Keywords:
Microporous organic polymer
Polymer of intrinsic microporosity (PIM-1)
Fumed silica nanoparticle
Nanocomposite
Mixed-matrix
Gas permeability

ABSTRACT

Recently, high-free volume, glassy ladder-type polymers, referred to as polymers of intrinsic microporosity (PIM), have been developed and their reported gas transport performance exceeded the Robeson upper bound trade-off for O_2/N_2 and CO_2/CH_4. The present work reports the gas transport behavior of PIM-1/silica nanocomposite membranes. The changes in free volume, as well as the presence and volume of the void cavities, were investigated by analyzing the density, thermal stability, and nano-structural morphology. The enhancement in gas permeability (*e.g.*, He, H_2, O_2, N_2, and CO_2) with increasing filler content shows that the trend is related to the true silica volume and void volume fraction.

1. Introduction

As a means of modifying gas transport properties in glassy polymer membranes, Pinnau and He first reported an unexpected increase of gas permeability in a series of high-free-volume glassy polymers whereby inorganic non-porous nanoparticles, such as fumed silica or carbon black, were incorporated into the polymeric matrix to change the inherent polymer chain packing [1]. Subsequent studies [2–4] have shown that the gas permeability of non-porous inorganic (*e.g.*, fumed silica, MgO, TiO_2)-filled glassy polymeric mixed-matrix membranes do not behave according to the Maxwell [5] and other proposed models [6,7], which predict lower gas permeabilities than in unfilled polymers. Especially, nanosized non-porous fumed silica particles embedded in glassy polymer matrices have a tendency to form aggregates, which result in disruption of polymer packing and the creation of void spaces. Because of the resulting increase in free volume, the gas permeabilities generally increase with silica content, whereas the selectivities for permanent gases, such as oxygen/nitrogen, are concurrently compromised. This phenomenon has been investigated and confirmed in our previous study [8] through the addition of silica nanoparticles in conventional low-free-volume polysulfone. It has been observed [9,10] that the relative permeability (*i.e.*, the ratio of permeability of silica-filled polymer to that of unfilled polymer) increased with the penetrants' molecular size, leading to a considerable decrease in the selectivity of gas pairs such as O_2/N_2 and CO_2/CH_4. More importantly, the trend of an increase in relative permeability is substantially influenced by the silica nanoparticle loadings that may have arisen from the nonlinearly expanded free volume due to the enhanced aggregates size as silica content increases. The addition of fumed silica to increase the gas permeability of the resulting nanocomposites was initially applied using high-free-volume glassy polymers such as poly(4-methyl-2-pentyne) (PMP), poly(1-trimethylsilyl-1-propyne) (PTMSP), and the perfluoropolymer Teflon AF2400 [11–13]. In these polymers, the incorporation of nanoparticles led to increases in gas and vapor permeability and, also enhanced reverse selectivity behavior for condensable C_{3+} hydrocarbons over smaller non-condensable gases, such as hydrogen or methane.

☆ NRCC Publication No. 51765. Presented in part at the 2008 International Congress on Membranes and Membrane Processes (ICOM), Honolulu, Hawaii, July 12–18, 2008.

* Corresponding author at: Institute for Chemical Process and Environmental Technology, National Research Council of Canada, 1200 Montreal Road, Ottawa, ON K1A 0R6, Canada. Tel.: +1 613 993 9753; fax: +1 613 991 2384.
E-mail address: michael.guiver@nrc-cnrc.gc.ca (M.D. Guiver).

0376-7388/$ – see front matter.
doi:10.1016/j.memsci.2009.09.047

Tailoring free-volume cavities by controlling the size and shape of microporous polymers is directly related to the gas permeation properties [14]. In particular, PIM ladder polymers are good potential candidates with the capability to optimize the gas permeability and selectivity by changing the polymer chain packing [15]. Budd et al. and McKeown et al. were the first to report this new class of rigid ladder-type polydioxanes containing highly contorted chains and defined them as polymers of intrinsic microporosity (PIM) [16,17]. Among these novel materials, PIM-1, containing the contorted spirobisindane unit, has attracted the most attention due to its relative ease of synthesizing high molecular weight polymer and the combination of outstanding permeability with moderate selectivity, especially for O_2/N_2 and CO_2/CH_4 pairs, which overcome the upper bound trade-off proposed by Robeson [18,19]. Since the initial reports of Budd et al. and McKeown et al., structurally new PIMs and additional data on PIM-1 have appeared [20–25].

In the present study, fumed silica nanoparticles were incorporated into PIM-1, and the resulting gas permeation properties of the mixed-matrix nanocomposite membranes were investigated. Pure-gas permeability data are reported for He, H_2, O_2, N_2, and CO_2 of the PIM-1 nanocomposite membranes and compared with unfilled PIM-1. The effects on the changes in thermal properties as well as the morphology including particle distribution and aggregation by the addition of fumed silica are discussed. In addition, the trend of the resulting permeability-selectivity trade-off relationship of PIM-1/silica nanocomposites is evaluated.

2. Background

2.1. The effect of impermeable inorganic filler on density and void volume

The filler volume fraction of a polymeric membrane containing non-porous inorganic particles is determined by Eq. (1):

$$\phi_F = \frac{w_F/\rho_F}{w_P/\rho_P + w_F/\rho_F} \quad (1)$$

where w_F and w_P refer to the weight of filler and polymer, respectively, and ρ_F and ρ_P are the density of filler and polymer, respectively. The density of the nanocomposites can be predicted using Eq. (2):

$$\rho_{pred} = \rho_P(1-\phi_F) + \rho_F\phi_F \quad (2)$$

However, the density obtained by experimental measurements is typically somewhat lower than the predicted values. The difference between experimental (ρ_{exp}) and predicted density (ρ_{pred}), might be considered as the void space (ϕ_V) that exists at the interface of the polymer and silica nanoparticle aggregates or between the aggregates. The void volume fraction is determined by Eq. (3):

$$\phi_V = 1 - \frac{\rho_{exp}}{\rho_{pred}} \quad (3)$$

2.2. Gas transport properties of mixed-matrix nanocomposite membranes

Gas permeation in heterogeneous materials that contain impermeable spherical particles is commonly predicted by the Maxwell model [5] using Eq. (4):

$$P_C = P_P\left(\frac{1-\phi_F}{1+(\phi_F/2)}\right) \quad (4)$$

where P_C is the permeability of the composite medium and P_P is the permeability of the pure polymer.

3. Materials and methods

3.1. Materials

PIM-1 polymer was synthesized by polycondensation reaction of 5,5′,6,6′-tetrahydroxy-3,3,3′,3′-tetramethyl-1,1′-spirobisindane (TTSBI) with 2,3,5,6-tetrafluoro-terephthalonitrile (TFTPN) in dimethylacetamide (DMAc) [23,24]. The molecular weight (M_w) and molecular dispersity (M_w/M_n), determined by gel permeation chromatography (GPC) in THF against polystyrene standards, were approximately 100,000 Da and 2.9, respectively. Measured BET surface area for unfilled PIM-1 was 730 m^2/g. Hydrophobic fumed silica (Cabosil TS 530) containing trimethylsilyl groups was kindly supplied by Cabot Corporation (Tuscola, IL). The density and the BET surface area for Cabosil TS 530 are 2.2 g/cm^3 and 205–245 m^2/g, respectively [26]. The average equivalent spherical particle diameter (d) is approximately 11.1–13.3 nm, which was estimated by: $d = 6/(\text{surface area} \times \text{density})$ for spherical particles.

3.2. PIM-1 and silica nanoparticles filled-PIM-1 membranes preparation

Initially, polymer and fumed silica were thoroughly dried in a vacuum oven at 100 °C. 2 wt.% of PIM-1 was completely dissolved in chloroform (EMD Chemical Inc. Gibbstown, NJ). After filtering the polymer solution with a 0.45 μm pore size polypropylene syringe filter, the desired amount of silica nanoparticles, ϕ_F (*i.e.*, 7, 13, 19, and 24 vol.%) based on Eq. (1) was added in the solution. The solution-suspension was stirred with a magnetic bar for a minimum of 15 h, and up to 60 h for higher ϕ_F. The solution-suspension was poured into a leveled glass casting dish, which was then covered to reduce evaporation rate. After solvent evaporation, the resulting films were delaminated and conditioned by soaking in methanol for approximately 50 min. Immersing the membranes in methanol reverses prior film formation history, in a manner similar to protocols previously developed for microporous polyacetylenes and PIM-1 [27,28]. After leaving the films under ambient atmospheric conditions for 1 h, the films were dried in a vacuum oven at 100 °C for 2 days. The thickness of the membranes was measured with a micrometer, and was in the range of 35–55 μm.

3.3. Thermal gravimetric analysis

Thermal degradation was conducted by thermal gravimetric analysis (TGA) (TA instrument 2950, TA Instruments, New Castle, DE). Samples of approximately 3–6 mg were loaded into platinum pans and tested under a 50 mL/min purge of nitrogen gas. Initially, the samples were heated up to 350 °C at a rate of 10 °C/min. After cooling to room temperature, the sample was reheated up to 1000 °C at a rate of 10 °C/min.

3.4. Differential scanning calorimetry

Glass transition temperatures (T_g) were determined by differential scanning calorimetry (DSC) (TA Instruments 2920, TA Instruments, New Castle, DE) calibrated by tin (231.93 °C) and zinc (419.53 °C). The samples were tested under a 50 mL/min purge of nitrogen gas. Samples of approximately 10 mg were encapsulated in the non-hermetically sealed aluminum pans and lids. Samples were initially heated from room temperature up to 400 °C at a rate of 10 °C/min. After quenching in liquid nitrogen, the samples were reheated up to 450 °C at a rate of 10 °C/min.

3.5. Scanning electron microscopy

The cross-section and surface morphology of mixed-matrix nanocomposite membranes were observed by scanning electron

Table 1
Thermal properties.

ϕ_F (%)	w_F (%)	wL (%)	T_1 (°C)	T_5 (°C)	T_g (°C)
0.0	0	37.7	492	513	No
6.7	13	33.2	492	516	–
13.0	24	30.0	495	518	–
19.1	33	27.0	497	520	–
23.5	39	25.4	498	521	No
Fumed silica*	–	5.6	336	787	–

wL: weight loss up to 1000 °C.
T_1: temperature at 1% weight loss.
T_5: temperature at 5% weight loss.
T_g: glass transition temperature.
No: none observed.

microscopy (SEM). Rather unexpectedly, the silica-filled PIM-1 membrane samples were more readily fractured under ambient conditions, whereas they were more flexible in liquid N_2. The fractured membrane samples were sputter-coated with gold. The samples were then examined using a JEOL 840A scanning electron microscope equipped with an Oxford instruments 6560 INCA x-sight light element energy dispersive X-ray (EDX) spectrometer and image capturing software. All photos were taken using an accelerating voltage of 30 kV.

3.6. Gas permeation measurements

The pure-gas permeability was measured using a constant pressure/variable volume apparatus [29]. The feed gas pressure was maintained at 50 psig while the permeation side was kept at atmospheric pressure (0 psig). The gas permeation measurements were performed at 23 ± 0.2 °C in the following order: O_2, N_2, He, H_2, and CO_2. The permeate gas flow rate was measured by a soapfilm bubble flowmeter (Grace, IL). The gas permeability (P) was calculated by the following equation (Eq. (5)):

$$P = \frac{273}{T}\frac{dV}{dt}\frac{l}{\Delta p \cdot A} \quad (5)$$

where dV/dt is the volumetric flow rate, T is the operational temperature (K), A is the active permeation membrane area (9.6 cm^2), l is the thickness of the membrane, and Δp is the pressure difference between feed side and permeation side. The permeability is reported in Barrer [10^{-10} cm^3 (STP) cm/cm^2 s cmHg].

4. Results and discussion

4.1. DSC and TGA

The amorphous PIM-1 and PIM-1/silica nanocomposites remain in the glassy state until the polymer decomposition point; hence, no thermal transition was observed up to 420 °C by the DSC analysis. Because of the lack of rotational mobility in the backbone of the rigid ladder polymer, it is difficult to observe a glass transition before degradation [20]. Although PIM-1 has been reported as having a T_g, 436 °C [21], we believe this appears to be a probable misinterpretation of the data. Table 1 presents the weight loss of various wt.% of fumed silica mixed-matrix membranes at temperatures up to 1000 °C. During TGA analysis, the initial weight of the samples was affected by buoyancy; that is, the sample and platinum pan appeared to gain weight before significant decomposition occurred due to the differences in thermal conductivity, density, and heat capacity for the purging gas and the sample [30]. However, the buoyancy effect was less apparent at higher temperature. Thus, the initial wt.% for all the samples was set at 350 °C. The silica concentration in the polymer (ϕ_F) is considered as the volume fraction, which appears significantly lower than the weight fraction term because of the high density of fumed silica. PIM-1 and all nanocomposites began weight loss at approximately 492 °C. The weight loss temperature at 1% (T_1) and 5% (T_5) slightly increased with ϕ_F, indicating a higher thermal stability by the addition of silica nanoparticles [31]. It is believed that initial decomposition is the result of the loss of trimethylsilyl groups present in the modified fumed silica.

4.2. Microporous morphology

The silica-nanoparticle-filled PIM-1 membranes were observed by SEM. Fig. 1 presents the cross-sectional morphological images

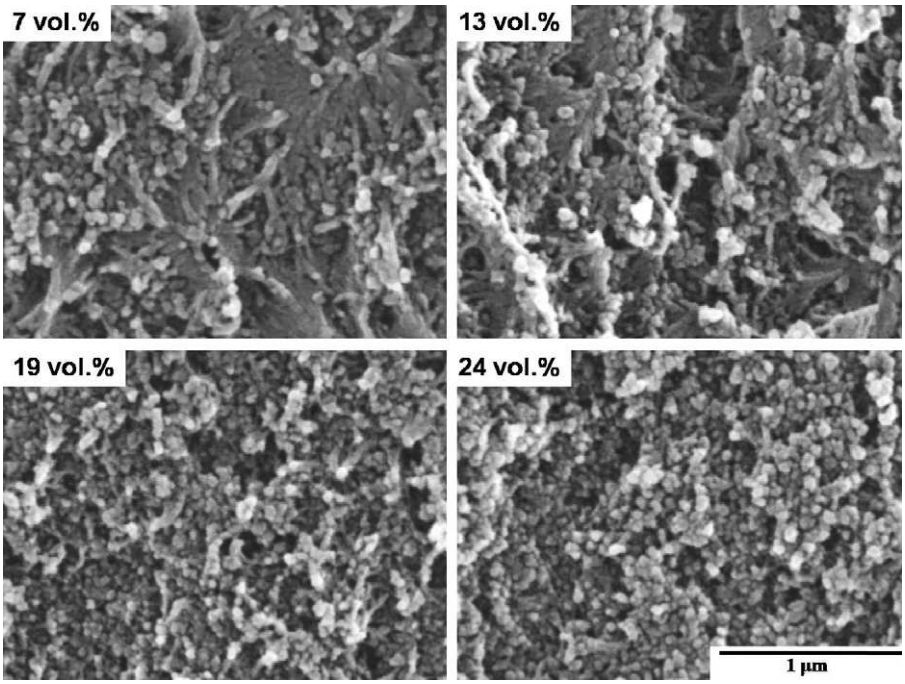

Fig. 1. SEM images of the cross-section of silica-filled PIM-1 mixed-matrix membranes with various amounts of silica nanoparticle loadings (magnification 50,000×).

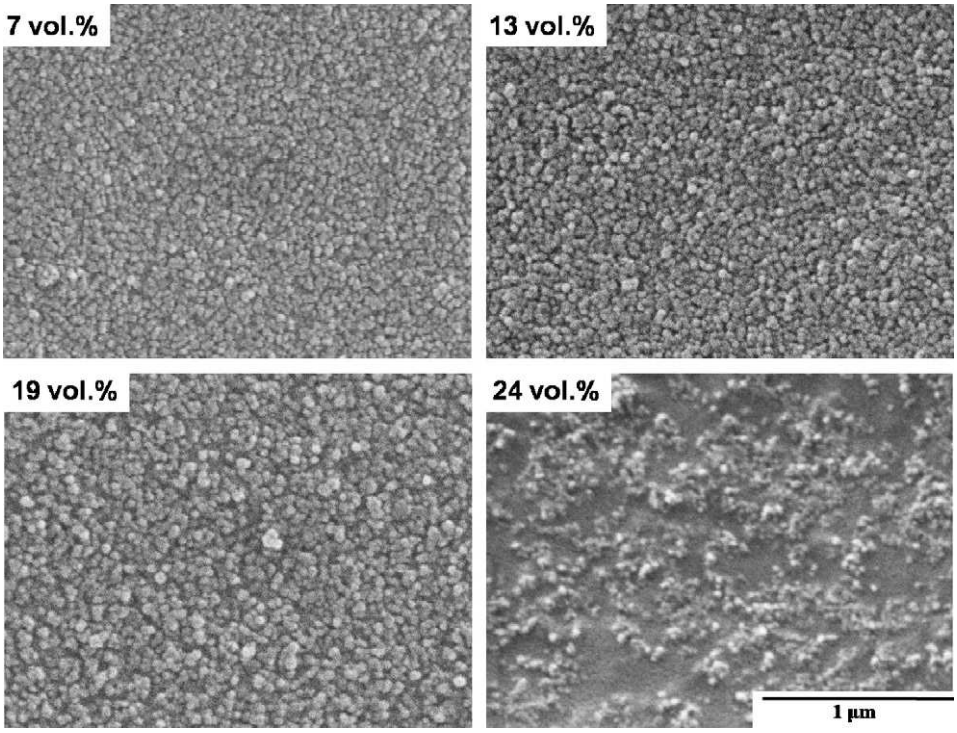

Fig. 2. SEM images of the surface of silica-filled PIM-1 mixed-matrix membranes with various amounts of silica nanoparticle loadings (magnification 50,000×).

of silica embedded PIM-1 mixed-matrix membranes, showing that the non-porous silica nanoparticles are aggregated rather than dispersed individually [32]. Fig. 2 clearly shows that the size (*e.g.*, diameter) of nanoparticle aggregates increases as ϕ_F increases, whereas the number of aggregate clusters decreases. In principle, the interparticle spacing should decrease with increasing particle loading, if the particle size is constant [33]. However, inter-aggregate spacing is created between nanoparticle aggregates, which become bigger at higher particle concentration. Therefore, additional void volume besides fractional free volume exists in the microporous PIM-1 polymer matrices. Consequently, the size of the aggregates plays a key role in the gas permeation properties due to the formation of void space in the nanocomposites [34].

The aggregates formed within the 24 vol.% of silica-filled membranes are somewhat different from those containing lesser amounts. Moreover, the diameter of aggregates is obviously large, approximately over 200 nm. The aggregate shape is clearly non-uniform compared with the others that appear better dispersed and have a more uniform aggregate size. It is noteworthy that the relative permeability is almost identical for the nanocomposite membranes containing less than 20 vol.% silica, indicating that the local flow pattern around a filler particle is not disturbed by the presence of other particles [6].

4.3. Density and void volume

The presence of void volume can be demonstrated by the difference between the theoretical and measured density. In theory, when two different materials are dispersed and blended together, the density of the resulting composite material is ideally calculated by Eq. (2). However, in practice, the density of nanocomposites composed of embedded inorganic non-porous fillers in glassy polymers tends to be lower than the calculated density as shown in Table 2. The density was measured by gravimetric analysis (*i.e.*, samples of known area and thickness were weighed on an analytical balance). This is because significant void space can be created at the interface between polymer and silica aggregates or within nanosized aggregates [9,35]. Therefore, the packing density of silica-filled PIM-1 membranes is lower than the theoretically expected value.

Fig. 3 presents the differences in experimentally measured density (ρ_{exp}) and predicted results (ρ_{pred}) as a function of ϕ_F. For the nanocomposite membrane containing the low silica loading ϕ_F of 7 vol.%, ρ_{exp} appears to follow ρ_{pred}. On the other hand, ρ_{exp} shows a significant drop at high silica loadings and the differences between ρ_{exp} and ρ_{pred} become significant as ϕ_F increases. Previously, this phenomenon has been observed for nanocomposites of embedded TiO_2 nanoparticles within PTMSP [3].

Fig. 4 presents the relationship of the void volume with added silica amounts as calculated by Eq. (3). The void volume increases linearly with increasing silica content, but above 7 vol.% of silica, a marked nonlinear behavior is observed. This is significant in explaining the changes in gas permeability, which will be discussed later. In polymer/inorganic mixed-matrix membranes, the total volume fraction (ϕ_T) is the sum of ϕ_F, ϕ_P, and ϕ_V. Considering the occurrence of ϕ_V, the true silica volume (ϕ_F^T) in nanocomposites

Table 2
Physical properties of PIM-1 and PIM-1/silica mixed-matrix membranes.

ϕ_F (%)	ρ_{exp} (g/cm^3)	ρ_{pred} (g/cm^3)	ϕ_V (%)	ϕ_F^T (%)
0.0[a]	1.056	–	–	–
0.0	0.991	0.991	–	–
6.7	1.070	1.064	−0.6[b]	6.8
13.0	1.092	1.131	3.4	12.5
19.1	1.084	1.197	9.4	17.3
23.5	1.069	1.244	14.0	20.0

ρ_{exp}: experimental density.
ρ_{pred}: theoretical density.
ϕ_F: silica volume fraction.
ϕ_V: void volume fraction.
ϕ_F^T: true silica volume fraction.
[a] Without methanol treatment.
[b] Negative value is attributed to the range of experimental error.

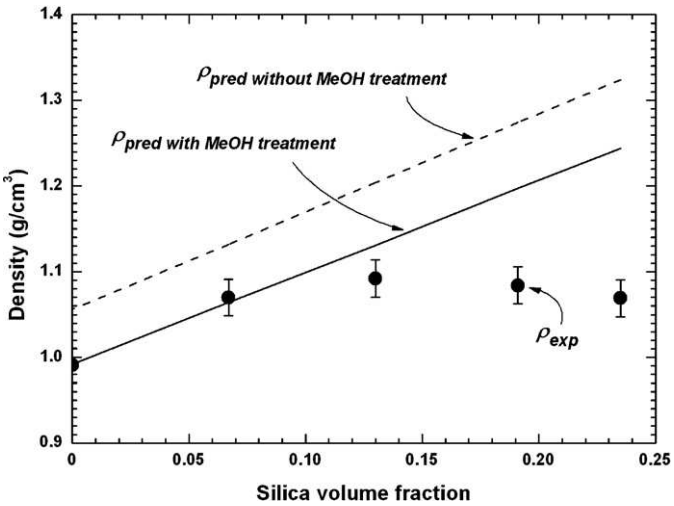

Fig. 3. The measured and calculated density determined by Eq. (2); the dotted line is the predicted density of the film without methanol treatment, the solid line is the predicted density of the film treated by methanol, and the circles are the experimentally measured densities of each sample (error range of ±3%).

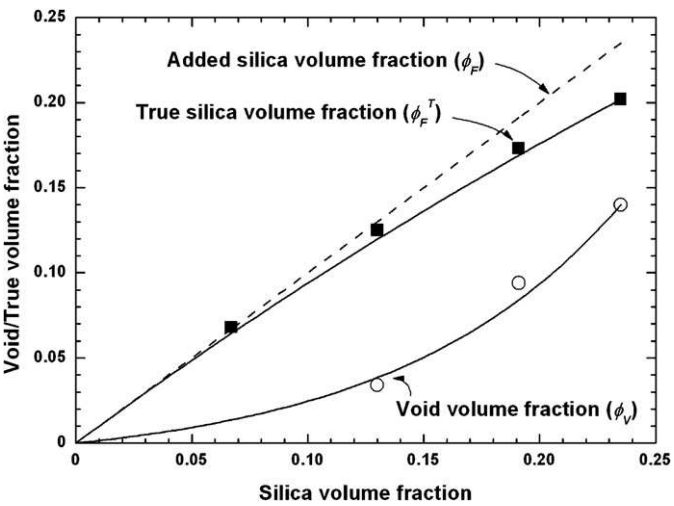

Fig. 4. Void volume (○) and true silica volume fraction (■) filled in matrix derived by Eq. (3) and Eq. (6), respectively; the dotted line is the theoretically estimated silica volume fraction.

can be calculated by Eq. (6):

$$\phi_F^T = \phi_F(1 - \phi_V) \quad (6)$$

The differences between ϕ_F^T and ϕ_F increased with silica loading, and became larger due to the presence of high void volume resulting from aggregation at higher ϕ_F, as presented in Fig. 5. This nonlinear increase in void volume with increasing ϕ_F is probably related to the formation of larger irregular aggregates in the matrix filled with the maximum concentration of fumed silica.

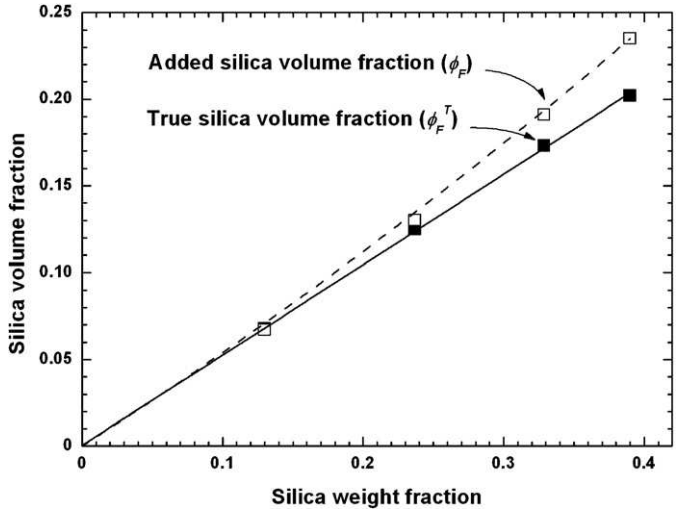

Fig. 5. The originally added silica volume fraction (□) and actual added silica volume fraction (■) related to the silica weight fraction.

4.4. Gas permeation properties of PIM-1

In highly rigid glassy polymers, the transport properties can vary with the film formation procedures [36]. Accordingly, the gas transport properties of PIM-1 are considerably influenced by various film formation and treatment protocols including casting solvent type and drying conditions [22]. Table 3 presents the gas permeabilities and selectivities of PIM-1 membranes, which were prepared by various solvents (*e.g.*, tetrahydrofuran (THF), dichloromethane (DCM), and chloroform) and treated by immersion in water or methanol. Treatment of PIM-1 membranes with methanol was used to remove prior membrane formation history. The gas permeability of PIM-1 post-treated with methanol increased approximately 2-fold. The gas permeability of PIM-1 decreases in following order:

$$CO_2 \gg H_2 \gg O_2 > He \gg N_2$$

This behavior is similar to that of other high-free-volume glassy polymers, such as substituted polyacetylenes. Compared to low-free-volume polymers, such as polysulfone, PIM-1 and substituted polyacetylenes have a large fraction of interconnected free volume elements, which allow for high diffusion coefficients as well as high gas solubility [37,38].

4.5. Gas permeation properties of PIM-1/silica mixed-matrix membranes

The gas permeation properties of the nanocomposites as a function of silica loading are shown in Table 4. Composite membranes

Table 3
Gas permeability properties of PIM-1 films prepared by different methods.

Casting solvent^{treatment}	Gas permeability, *P* (Barrer)						Selectivity		Temp. (°C)	Δ*p* (psig)	Reference
	He	H_2	O_2	N_2	CH_4	CO_2	O_2/N_2	CO_2/N_2			
Tetrahydrofuran	–	1300	370	92	125	2,300	4.0	25	30	2.9	Budd [20]
Dichloromethane	1060	2330	790	240	360	3,500	3.3	15	35	58.8	Staiger [21]
Chloroform	760	1630	580	180	310	4,390	3.2	24	25	14.7	Budd [22]
Chloroform^{water}	–	–	150	45	114	1,550	3.3	34	25	14.7	Budd [22]
Chloroform^{MeOH}	–	–	1610	500	740	12,600	3.2	25	23	14.7	Budd [22]
Chloroform^{MeOH}	1500	3600	1300	340	430	6,500	3.8	19	25	50.0	Thomas [23]
Chloroform^{MeOH}	–	1900	990	270	350	4,030	3.7	15	25	50.0	Song [24]
Chloroform^{MeOH}	1380	3320	1340	405	–	6,000	3.3	15	25	50.0	This study

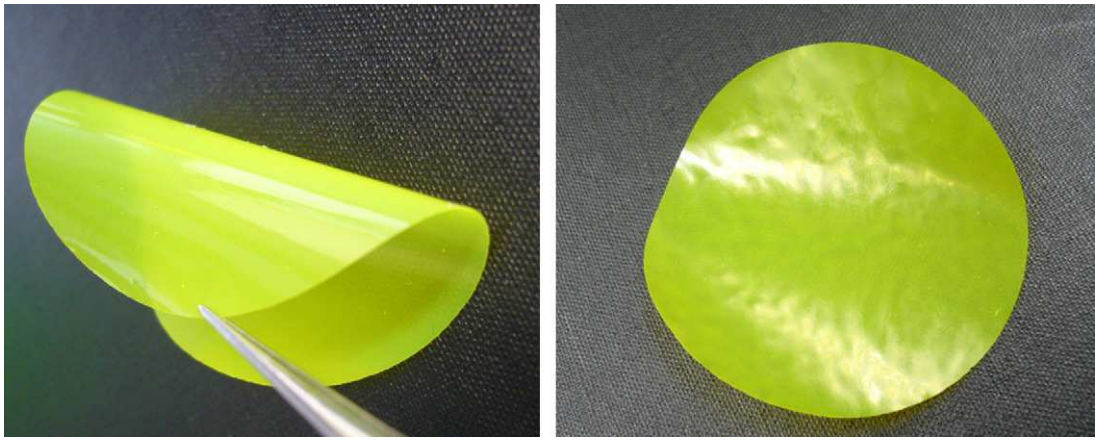

Fig. 6. Images of PIM-1/24 vol.% silica mixed-matrix membrane; note the absence of apparent defects, with particles well dispersed in the polymeric matrix.

Table 4
Gas permeability properties of PIM-1 and fumed silica-filled nanocomposites as a function of silica loadings.

ϕ_F (%)	Gas permeability (Barrer)					Selectivity	
	He	H_2	O_2	N_2	CO_2	O_2/N_2	CO_2/N_2
0.0	1380	3320	1340	405	6,000	3.3	15.0
6.7	1540	3670	1480	460	6,200	3.2	15.0
13.0	2000	5060	2330	880	10,100	2.7	12.0
19.1	2518	6362	3221	1573	12,182	2.1	7.8
23.5	2940	7190	3730	1800	13,400	2.1	7.5

having more than 30 vol.% silica nanoparticles were brittle. For this reason, the amount of dispersed silica nanoparticles was limited to a maximum of 24 vol.%, which resulted in flexible nanocomposite membranes as shown in Fig. 6. The gas permeabilities generally increased with ϕ_F, which is in contrast with the prediction of the Maxwell model.

Fig. 7 presents the enhanced relative permeability of each single gas measured at 25 °C and Δp of 50 psig as a function of ϕ_F^T. Matteucci et al. [39,40] described that the existence of void volume (*i.e.*, macrovoids) at the nanoparticle–polymer interface, between nanoparticle aggregates, or as a result of nanoparticle-induced disruption of polymer chain packing is barely distinguishable. However, it leads to the enhancement of gas permeability. In addition, it is observed that the mode of the enhanced permeability with ϕ_F^T significantly follows the trend of ϕ_V with increasing ϕ_F. As discussed above, the ϕ_V increases nonlinearly with ϕ_F, and presumably the relative permeability is consistent with ϕ_V.

Fig. 8 presents the increasing relative permeability as a function of ϕ_V. The permeability enhancement behaves nonlinear with increasing ϕ_V, which could be attributed to the increase in particle loadings in the membrane. However, the enhancement in permeability tends to stabilize with increased loadings.

The trade-off relationship between O_2 permeability and O_2/N_2 selectivity of several polymers is presented in Fig. 9. It is evident that incorporating silica nanoparticles into glassy polymer matrices leads to increases in gas permeabilities in both low-free-volume polysulfone and high-free-volume PIM-1. However, the selectivity decreases with increased silica nanoparticle loadings and the general trend of the PIM-1/silica nanocomposites follow approximately the profile of the upper bound limit.

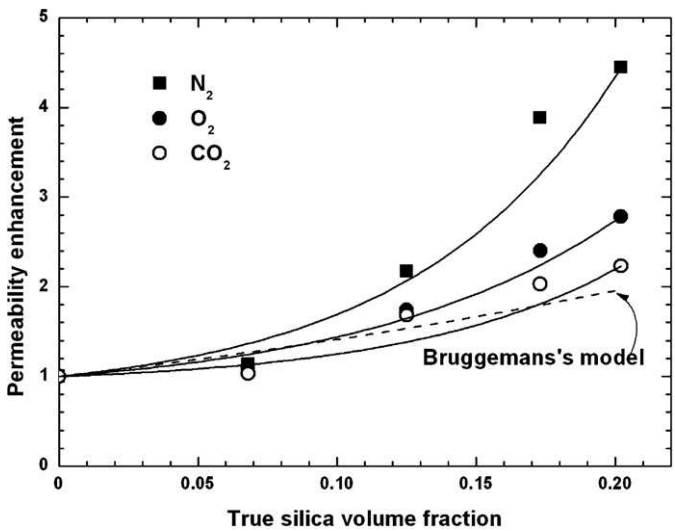

Fig. 7. Gas permeability of N_2 (■), O_2 (●), and CO_2 (○) influenced by the incorporation of silica nanoparticles relative to that in unfilled PIM-1 membrane as a function of true silica volume fraction; properties were measured at 25 °C and Δp of 50 psig after being soaked in methanol and dried at 100 °C in a vacuum oven; the dotted line represents highly permeable dispersed phase by the Bruggeman's model [6].

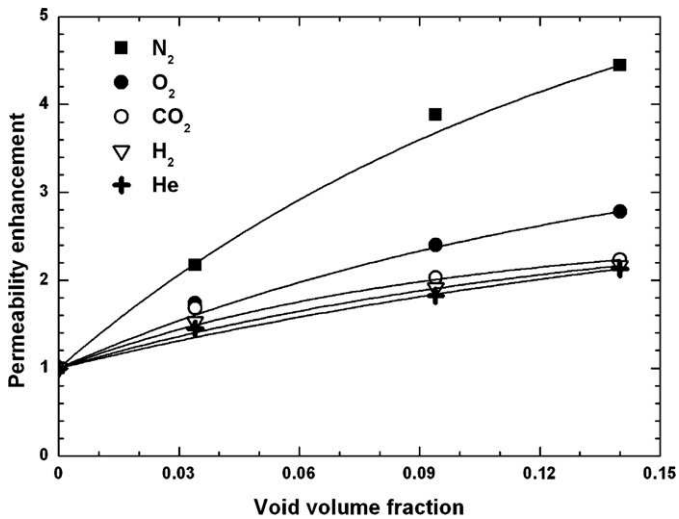

Fig. 8. Gas permeability of H_2 (▽), He (✚), N_2 (■), O_2 (●), and CO_2 (○) influenced by the incorporation of silica nanoparticles relative to that in unfilled PIM-1 membrane as a function of void volume fraction; properties were measured at 25 °C and Δp of 50 psig after being soaked in methanol and dried at 100 °C in a vacuum oven.

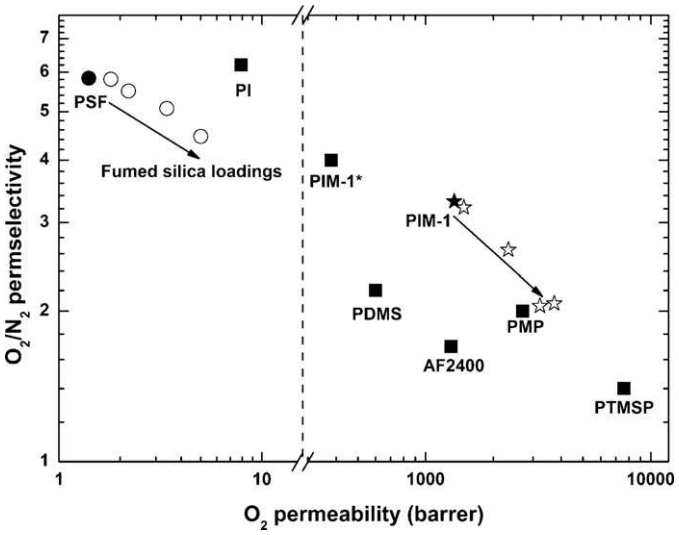

Fig. 9. The trade-off performance for gas permeability and selectivity through conventional, low-free-volume glassy polysulfone (PSf), polyimide (PI), high-free-volume glassy poly(4-methyl-2-pentyne) (PMP), poly(1-trimethylsilyl-1-propyne) (PTMSP), poly(2,2-bis(trifluoromethyl)-4,5-difluoro-1,3-dioxole-*co*-tetrafluoroethylene) (Teflon AF2400), rubbery polydimethylsiloxane (PDMS), and PIM-1 (PIM-1* refers to a literature value [20]). Open circles and stars show the results of nanocomposites with fumed silica at various loadings.

5. Conclusions

PIM-1/fumed silica mixed-matrix membranes were successfully prepared with various levels of silica nanoparticle loadings to investigate the gas transport performance. The specific relationship of void space with silica nanoparticle content was investigated by determining the true silica volume fraction as well as void volume fraction. The incorporation of silica nanoparticles in PIM-1 significantly increased overall gas permeability. This is likely because significant increases in the newly created void cavities upon the addition of impermeable nanoparticles was greater than the permeable space of the unfilled polymer chain packing. In addition, the trend of increased permeability increases nonlinearly with the amount of silica content. The trade-off relationship between O_2 permeability and O_2/N_2 selectivity followed a similar trend previously observed for polysulfone mixed-matrix membranes with incorporated silica nanoparticles, whereby permeability was gained at the expense of selectivity.

Acknowledgements

The authors gratefully acknowledge a Manpower Development Program for Energy & Resources Grant supported by the Ministry of Knowledge and Economy (MKE) (2008EAPHMP1700002008). This work was partially supported by the Climate Change Technology and Innovation Initiative, Greenhouse Gas project (CCTII, GHG), Natural Resources Canada (NRCan). We thank David Kingston of the National Research Council for performing SEM measurements.

References

[1] I. Pinnau, Z. He, Filled superglassy membrane, US Patent 6,316,684 (2001).
[2] H. Lin, S. Matteucci, B.D. Freeman, S. Kalakkunnath, D.S. Kalika, Novel membrane materials for CO_2 removal from mixtures with H_2, Prep. Symp. Am. Chem. Soc. Div. Fuel Chem. 50 (2005) 617.
[3] S. Matteucci, V.A. Kusuma, D. Sanders, S. Swinnea, B.D. Freeman, Gas transport in TiO_2 nanoparticle-filled poly(1-trimetylsilyl-1-propyne), J. Membr. Sci. 307 (2008) 196.
[4] S.S. Hosseini, Y. Li, T.-S. Chung, Y. Liu, Enhanced gas separation performance of nanocomposite membranes using MgO nanoparticles, J. Membr. Sci. 302 (2007) 207.
[5] C. Maxwell, Treatise on Electricity and Magnetism, Oxford Univ. Press, London, 1873.
[6] R.H.B. Bouma, A. Checchetti, G. Chidichimo, E. Drioli, Permeation through a heterogeneous membrane: the effect of the dispersed phase, J. Membr. Sci. 128 (1997) 141.
[7] R. Pal, Permeation models for mixed matrix membranes, J. Colloid Interface Sci. 317 (2008) 191.
[8] J. Ahn, W.-J. Chung, I. Pinnau, M.D. Guiver, Polysulfone/silica nanoparticle mixed-matrix membranes for gas separation, J. Membr. Sci. 314 (2008) 123.
[9] S. Takahashi, D.R. Paul, Gas permeation in poly(ether imide) nanocomposite membranes based on surface-treated silica. Part 1. Without chemical coupling to matrix, Polymer 47 (2006) 7519.
[10] S. Takahashi, D.R. Paul, Gas permeation in poly(ether imide) nanocomposite membrane based on surface-treated silica. Part 2. With chemical coupling to matrix, Polymer 47 (2006) 7535.
[11] T.C. Merkel, B.D. Freeman, R.J. Spontak, Z. He, I. Pinnau, P. Meakin, A.J. Hill, Ultrapermeable, reverse-selective nanocomposite membranes, Science 296 (2002) 519.
[12] T.C Merkel, Z. He, I. Pinnau, B.D. Freeman, P. Meakin, A.J. Hill, Effect of nanoparticles of gas sorption and transport in poly(1-trymethylsilyl-1-propyne), Macromolecules 36 (2003) 6844.
[13] T.C. Merkel, Z. He, I. Pinnau, B.D. Freeman, P. Meakin, A.J. Hill, Sorption and transport in poly(2,2-bis(trifluoromethyl)-4,5-difluoro-1,3-dioxole-co-tetrafluoroethylene) containing nanoscale fumed silica, Macromolecules 36 (2003) 8604.
[14] H.B. Park, C.H. Jung, Y.M. Lee, A.J. Hill, S.J. Pas, S.T. Mudie, E.V. Wagner, B.D. Freeman, D.J. Cookson, Polymers with cavities tuned for fast selective transport of small molecules and ions, Science 318 (2007) 254.
[15] C.M. Zimmerman, W.J. Koros, Polypyrrolones for membrane gas separation. 1. Structural comparison of gas transport and sorption properties, J. Polym. Sci. Polym. Phys. 37 (1999) 1235.
[16] N.B. McKeown, P.M. Budd, K. Msayib, B. Ghanem, Microporous polymer material, International patent, WO05012397 (2005).
[17] N.B. McKeown, S. Makhseed, Organic microporous materials, International patent, WO03000774 (2003).
[18] N.B. McKeown, P.M. Budd, Polymers of intrinsic microporosity (PIMs): organic materials for membrane separations, heterogeneous catalysis and hydrogen storage, Chem. Soc. Rev. 35 (2006) 675.
[19] N.B. McKeown, P.M. Budd, K. Msayib, B. Ghanem, Microporous polymer material, US Patent Appl. 20060246273 (2006).
[20] P.M. Budd, K.J. Msayib, C.E. Tattershall, B.S. Ghanem, K.J. Reynolds, N.B. McKeown, D. Fritsch, Gas separation membranes from polymers of intrinsic microporosity, J. Membr. Sci. 251 (2005) 263.
[21] C.L. Staiger, S.J. Pas, A.J. Hill, C.J. Cornelius, Gas separation, free volume distribution, and physical aging of a highly microporous spirobisindane polymer, Chem. Mater. 20 (2008) 2606.
[22] P.M. Budd, N.B. McKeown, B.S. Ghanem, K.J. Msayib, D. Fritsch, L. Starannikova, N. Belov, O. Sanfirova, Y. Yampolskii, V. Shantarovich, Gas permeation parameters and other physicochemical properties of a polymer of intrinsic microporosity: polybenzodioxane PIM-1, J. Membr. Sci. 325 (2008) 851.
[23] S. Thomas, I. Pinnau, N. Du, M.D. Guiver, Pure- and mixed-gas permeation properties of a microporous spirobisindane-based ladder polymer (PIM-1), J. Membr. Sci. 333 (2009) 125.
[24] J. Song, N. Du, Y. Dai, G.P. Robertson, M.D. Guiver, S. Thomas, I. Pinnau, Linear high molecular weight ladder polymers by optimized polycondensation of tetrahydroxytetramethylspirobisindane and 1,4-dicyanotetrafluorobenzene, Macromomolecules 41 (2008) 7411.
[25] N. Du, G.P. Robertson, J. Song, I. Pinnau, S. Thomas, M.D. Guiver, Polymers of intrinsic microporosity containing trifluoromethyl and phenylsulfone groups as materials for membrane gas separation, Macromolecules 41 (2008) 9656.
[26] CAB-O-SIL TS-530 Treated Fumed Silica: Technical Data, Cabot Corporation, 2004.
[27] K. Nagai, L.G. Toy, B.D. Freeman, M. Teraguchi, T. Masuda, I. Pinnau, Gas permeability and hydrocarbon solubility of poly[1-phenyl-2-[*p*-(triisopropylsilyl)phenyl]acetylene], J. Polym. Sci. Part B: Polym. Phys. 38 (2000) 1474.
[28] A.J. Hill, S.J. Pas, T.J. Bastow, M.I. Burgar, K. Nagai, L.G. Toy, B.D. Freeman, Influence of methanol conditioning and physical aging on carbon spin-lattice relaxation times of poly(1-trimethylsilyl-1-propyne), J. Membr. Sci. 243 (2004) 37.
[29] S.A. Stern, P.J. Gareis, T.F. Sinclair, P.H. Mohr, Performance of a versatile variable-volume permeability cell. Comparison of gas permeability measurements by the variable-volume and variable-pressure methods, J. Appl. Polym. Sci. 7 (1963) 2035.
[30] Buoyancy Phenomenon in TGA Systems, Thermal Analysis and Surface Solutions GmbH.
[31] D.Q. Vu, W.J. Koros, Mixed matrix membranes using carbon molecular sieves. 1. Preparation and experimental results, J. Membr. Sci. 211 (2003) 311.
[32] A. Chakrabarti, Effects of a fumed silica network on kinetics of phase separation in polymer blends, J. Chem. Phys. 11 (1999) 9418.
[33] J. Liu, H.-J. Schope, T. Palberg, An improved empirical relation to determine the particle number density of fluid-like ordered charde-stabilized suspensions, Part. Part. Syst. Charact. 17 (2000) 206.
[34] T.T. Moore, W.J. Koros, Non-ideal effects in organic–inorganic materials for gas separation membranes, J. Mol. Struct. 739 (2005) 87.

[35] R.J. Hill, Diffusive permeability and selectivity of nanocomposite membranes, Ind. Eng. Chem. Res. 45 (2006) 6890.
[36] M. Moe, W.J. Koros, H.H. Hoehn, G.R. Husk, Effects of film history on gas transport in a fluorinated aromatic polyimide, J. Appl. Polym. Sci. 36 (1988) 1833.
[37] V.P. Shantarovich, T. Suzuki, Y. Ito, K. Kondo, R.S. Yu, P.M. Budd, Y.P. Yampolskii, S.S. Berdonosov, A.A. Eliseev, Structural heterogeneity in glassy polymeric materials revealed by positron annihilation and other supplementary techniques, Phys. Stat. Sol. (c) 4 (2007) 3776.
[38] P.M. Budd, B. Ghanem, K. Msayib, N.B. McKeown, C. Tattershall, A nanoporous network polymer derived from hexaazatrinaphthylene with potential as an adsorbent and catalyst support, J. Mater. Chem. 13 (2003) 2721.
[39] S. Matteucci, V.A. Kusuma, S. Swinnea, B.D. Freeman, Gas permeability, solubility and diffusivity in 1,2-polybutadiene containing brookite nanoparticles, Polymer 49 (2008) 757.
[40] S Matteucci, V.A. Kusuma, S.D. Kelman, B.D. Freeman, Gas transport properties of MgO filled poly(1-trimethylsilyl-1-propyne) nanocomposites, Polymer 49 (2008) 1659.